Verification of a Spectrometer Breadboard for Characterization of a Future Spaceborne Sensor

Horst Schwarzer[1], Andreas Eckardt[1], and Ralf Reulke[2(✉)]

[1] DLR German Aerospace Center, Institute of Optical Sensor Systems, Rutherfordstraße 2, 12489 Berlin, Germany
andreas.eckardt@dlr.de
[2] Computer Vision, Humboldt-Universität zu Berlin, Unter den Linden 6, 10099 Berlin, Germany
reulke@informatik.hu-berlin.de

Abstract. German Aerospace Center **DLR** is involved in several hyperspectral missions for Earth remote sensing (e.g. EnMAP) but also for deep space and planetary missions (e.g. the Mercury mission Bepi Colombo). Hyperspectral instruments are designed for characterization of planetary surfaces, oceans and the atmosphere.

These spectrometers operate in the visible (VIS), near infrared (NIR), short wave infrared (SWIR) up to thermal infrared (TIR) spectral range with a spectral sampling below 10 nm up to 100 nm. In the spatial domain these instruments have more then 1000 pixels with a Ground Sampling Distance (GSD) of about 30 m up to 90 m.

The paper describes the calibration and performance verification of a breadboard model for future spectrometer on space-borne platforms. These procedures include measurements of the dark signal (DS), the linearity and deviation from linearity, noise behavior and signal to noise ratio (SNR) as well as photon transfer curve (PTC), the absolute radiometric calibration and the spectral imaging performance or the spectral resolution.

1 Introduction

In this paper the verification process of a breadboard solution (BB) for the DESIS instrument will be explained. An example for a space-borne instrument is DESIS (DLR Earth Sensing Imaging Spectrometer). This instrument will be installed on International Space Station (ISS). The instrument will be installed on the Multi-User System for Earth Sensing (MUSES) platform of Teledyne Brown Engineering.

DESIS was designed and developed to deliver precise data from the Earth surface and the atmosphere in the VIS/NIR spectral range with high spectral, high radiometric and moderate spatial resolution. To meet the sophisticated radiometric and spectral requirements and to guaranty a high reliability for detection of changes in the Earth ecosystem, a qualified in-flight calibration

F. Huang and A. Sugimoto (Eds.): PSIVT 2015 Workshops, LNCS 9555, pp. 285–295, 2016.
DOI: 10.1007/978-3-319-30285-0_23

concept including internal calibration, based on LED illumination and ground target based calibration have been established. A description of this instrument can be find in the paper from Eckardt [1].

With BB is to be shown that the test setup and the sensor is suitable in principle for the future measurement system on the Space Station.

This paper is organized as follows. Section 2 describes the DESIS hyperspectral imaging instrument. Section 3 introduces terminology and performance parameter, which has to be verified. Section 4 describes some measurements and their results. Finally, Sect. 5 presents our conclusions.

2 Instrument Description

DESIS is a hyperspectral instrument in a spectral range of 400 nm up to 1000 nm (VIS-NIR) and based on a modified Offner-Design for the Spectrometer. The telescope has a TMA (three-mirror anastigmat) design. Instead of the TMA, in the BB a telecentric glass-optics is used. The optical scheme of BB is shown in Fig. 1. The incoming light will be imaged by the objective into spectrometer slit plane. The slit defines the observed swath on the observed scene. The light enters the mirror and will be reflected onto the grating where the light is spectral dispersed and reflected back to the mirror. Then the mirror focuses the 2D spectrum of the scene into the focal plane of the spectrometer.

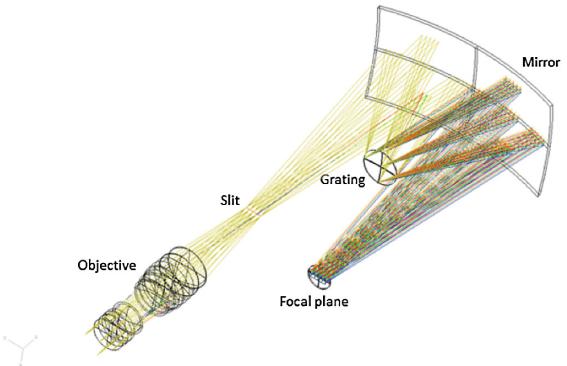

Fig. 1. Optical scheme of the BB

In the following Table 1 the design parameter of DESIS and BB are collected.

The DESIS-Detector is a sCMOS array. The pixel size is $24 \cdot 24\,\mu m^2$. 235 columns were used to perform the spectral channels and 1024 pixels (rows) were used in spatial direction. The radiometric resolution is 13 bit. A description of this detector can be found in the paper from Eckardt, [10].

For DESIS BB2 the GT3300 camera from Allied [8] was used. This camera is based on the Truesense KAI-08050 CCD-chip (see [9]).

Table 1. Optical performance data of DESIS and BB

	DESIS	DESIS BB
Telescope	2.8/320 mm	4/100 mm
FOV	4.4	7.6°
IFOV	0.004°	0.0074°
Spectrometer type	Offner	Offner
Spectral range	400 nm–1000 nm	450 nm–950 nm
Spectral channels	235	
Spectral sampling	2.55 nm	< 0.5 nm
In-orbit calibration	2 Internal LED field	2 internal lamps
Pointing (along-track)	±40°	

3 Radiometric Calibration

3.1 General Consideration

Overview about sensor performance consideration can be found in Kopeika [3], Janesick [4,5]. Following radiometric performance parameter are measured and derived for system verification.

- System gain determination (necessary for QE and DC determination)from Photon transfer curve (PTC),
- Linearity, saturation and non-linearity correction parameter,
- Signal to Noise Ratio (SNR),
- Dark Current (DC) and read noise measurements,
- Quantum efficiency (QE) determination.

3.2 Signal Calculation

The wavelength dependent incident radiance $L_{rad}(\lambda)$ causes irradiance $E(\lambda)$ on the detector chip ($f_{\#}$ is the f-number of the telescope, T_{opt}, R_{mir} and η_{gr} are the optics transmission, the Offner mirror reflection and grating efficiency):

$$E\left(\lambda\right) = \frac{\pi}{\left(4 \cdot f_{\#}^{2}\right)} \cdot T_{opt}\left(\lambda\right) \cdot R_{mir}^{2} \cdot \eta_{gr}\left(\lambda\right) \cdot L_{rad}\left(\lambda\right) \tag{1}$$

$< n_{ph} >$ is the average number of photons incident on the detector surface A_{pix} during integration time τ_{int}. $\cdot\eta_{disp}$ is the linear dispersion of the grating and defines the extent to which a spectral interval is spread out across a pixel in the focal plane (with the center wavelength λ) and is expressed in [nm/pixel].

$$\langle n_{ph} \rangle = \tau_{int} \cdot A_{pix} \cdot \eta_{disp} \cdot \frac{\lambda}{hc} \cdot E \tag{2}$$

The photons generate with a probability η_λ^{qu} electron - hole pairs in the semiconductor (quantum efficiency). This is the prerequisite for the stored electrons in the read-out register.

The measured digital gray value is s. It consists of the average (expectation-) value $\langle s \rangle$ and the noise.

$$s = \langle s \rangle + \eta_{DV} \cdot \left(\eta_V \cdot \left(\xi_{el} + \xi_{el}^D \right) + \xi_k \right) + \xi^{ADU} \tag{3}$$

The equation include the three noise- components: photon noise, dark current, and the read- or read-out noise. The last one are noise sources related to the sensor read out and amplifier circuits and can be described by a normal distribution with variance $\sigma_k^2 = \left\langle (\xi_k)^2 \right\rangle$. Photon noise and dark current are Poisson distributed.

The ADU noise (quantization noise) ξ^{ADU} will be neglected in this presentation. The average signal is

$$\langle s \rangle = \eta_{DV} \cdot \eta_V \cdot \eta_\lambda^{qu} \cdot \tau \cdot A_{pix} \cdot \eta_{gr} \cdot \frac{\lambda}{hc} \cdot E + DS \tag{4}$$

$\eta_{DV} \cdot \eta_V \cdot \left\langle n_{el}^D \right\rangle$ is the dark signal DS.

In this (linear) signal model the total variance σ_s^2 of the digital signal s is given according to the propagation of uncertainty (or propagation of error) by

$$\sigma_s^2 = \eta_{DV}^2 \cdot \eta_v^2 \cdot \left(\langle n_{el} \rangle + \left\langle n_{el}^D \right\rangle \right) + \eta_{DV}^2 \cdot \sigma_k^2. \tag{5}$$

With Eq. (4)

$$\langle s \rangle = \eta_{DV} \cdot \langle U \rangle = \eta_{DV} \cdot \eta_V \cdot \left(\langle n_{el} \rangle + \left\langle n_{el}^D \right\rangle \right)$$

Eq. (5) can be written in the following form:

$$\sigma_s^2 = \eta_{DV} \cdot \eta_V \cdot \langle s \rangle + \eta_{DV}^2 \cdot \sigma_k^2 \tag{6}$$

This linear equation is a relation between variance of measured noise and averaged signal. The slope is the system gain G_s and the offset is the read noise. The equation is related to the photon transfer method (see Janesick [5]) and can be use for characterization of the sensor.

3.3 Test Facility and Configuration

Experimental Setup was installed on an optical bench with a light-tight box. The measurements performed using a calibrated integrating sphere (IS) from Gigahertz Optics (see Fig. 2) with an output port diameter of 20 cm.The spatial homogeneity of the radiometric sphere is better than 1 %; the intensity stability is better than 0.06 % within 30 min The absolute radiometric calibration was provide by national metrological institute PTB. The irradiation level of this radiometric sphere can be varied over a large range by the shutters in front of the four Quartz Tungsten Halogen (QTH) lamps and additional metal filters

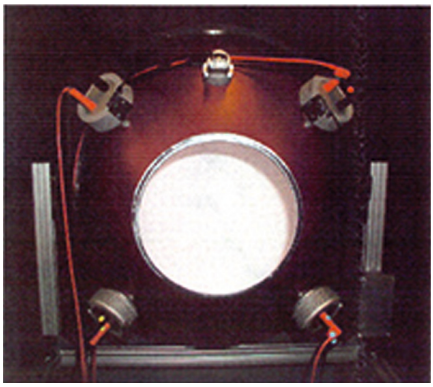

Fig. 2. Test setup for measuring the radiometric performance data with UMBB500var (IS) and interference filter (IF).

without changing the spectral behavior of the irradiation in contrast to current controlled radiometric spheres. This is essential for linearity measurements. The reference detector is a Hamamatsu.

The spectral performance measurements and calibrations will be performed using Penray lamps (e.g. from company **Newport**). To cover the spectral region from 400 nm to 1000 nm Hg, Ar, Ne and Kr spectral lamps were used.

4 Calibration and Performance Verification of BB

4.1 Photon Transfer Curve and Conversion Gain

The measurement concept is based on an analysis of detector signal and the corresponding noise by variation of input exposure (= irradiance x exposure time). With Eq. (6) the conversion gain can be derive from the slope between noise variance and signal. Figure 3 shows the result. The overall system (conversion) gain is 0.808 $[DN/e^-]$.

4.2 Linearity and Linearity Error

The principle of the measurement is to increase the incident exposure $E[i] = T_i \times E_0^i$ by changing either on the integration time (T_i) or the irradiance (E_0^i). Integration time can be measured with high accuracy and a large range of different T_i can be obtained. To test the entire measurement set-up the change of irradiance should also be taken into account. In this case the spectral behavior of the radiation source should not changes.

The straight line is a least squares fit. Below saturation (i.e. on the straight line part of the linearity plot), it can normally be arranged that the correlation coefficient between the data and the fitted line should normally be greater than e.g. 0.995.

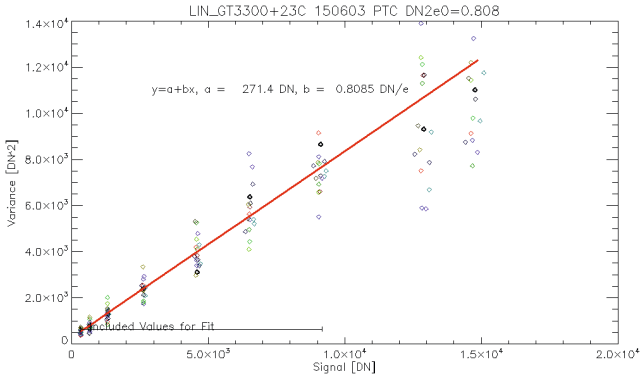

Fig. 3. Photon Transfer Curve. Results of the conversion gain determination and the error ranges.

Left Fig. 4 shows an example for the test results. The conversion gain was determined from PTC analyses as describes in the previous Sect. 4.1. The maximum signal of 2^{14} corresponds to $FWC = 20Te^{-}$. From the same data set the SNR can be derived (Fig. 4, right). A $SNR > 100$ can be realized with this detector for $DN \geq 10^4$.

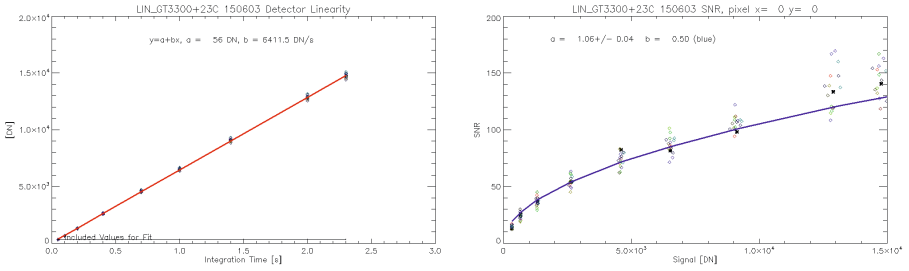

Fig. 4. Linearity and linear full well (left), SNR (right).

Non-linearity is significant, but can described by a polynomial fit. In the following figures (Fig. 5), non-linearity estimation are shown.

4.3 Dark Current

Dark current DC or dark current rate in $[e^{-}/pixel/sec]$ is calculated from averaged dark signal and is related to conversion gain and integration time.

With changing integration time, the dark signal noise rises. This relation is linear. In Fig. 6 the dark signal for different pixels is shown. The red line is a linear interpolation. The integration time range is from 0.1 s up to 2 s. To convert

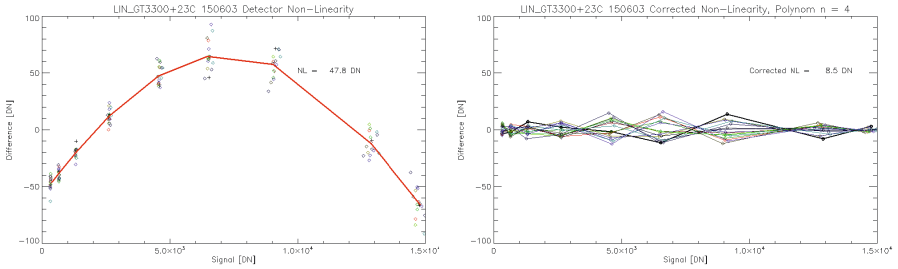

Fig. 5. Non-linearity (left) and and polynomial based correction (right). The remaining error is less than 1 %.

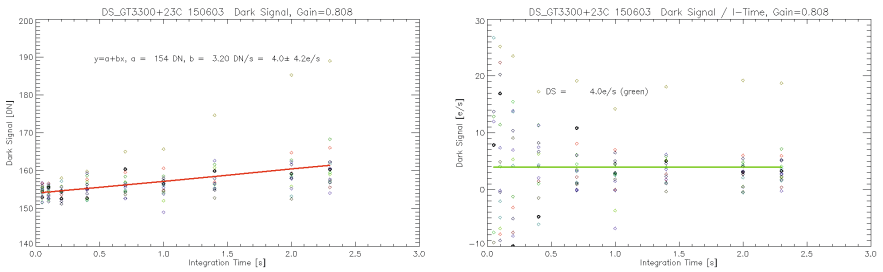

Fig. 6. Dark signal (left) and dark current (right) behavior for varying integration time at different locations on the chip. Dark current is 4 e/p/s or 2.1 pA/cm^2.

dark signal D_R from $[e/p/s]$ to $[pA/cm^2]$ we use the following equations ($Q = 1.6 \cdot 10^{-19}$ and $A = 5.5 \cdot 5.5\mu\text{m}^2$):

$$D_R\,[e/p/s] = \frac{J_d\,[A/cm^2] \cdot A\,[cm^2]}{Q} \quad J_d\,[A/cm^2] = \frac{Q \cdot D_R\,[e/p/s]}{A\,[cm^2]} \tag{7}$$

4.4 Spectral Responsivity and Quantum Efficiency (QE)

Spectral Responsivity is the ratio of measured signal (with substracted dark signal) to incident illumination measured in various spectral bands (responsivity measurement). A comprehensive curve gives the shape of the responsivity in a broad spectrum containing each measured spectral band.

The *quantum efficiency* (QE) at a given wavelength expressed as a percentage is the ratio of the number of photoelectrons at the detector output (signal with subtracted dark signal) to the number of incident photons in a given integration time.

The QE is measured at various wavelengths using narrow band filters. QE is being calculated using the formula (4) [%] and G_s from Subsect. 4.1. The description of the variables and constants can be found in Subsect. 3.2.

$$\eta_\lambda^{qu} = \frac{(\langle s \rangle - DS) \cdot h \cdot c}{G_S \cdot \tau_{\text{int}} \cdot E \cdot A_{pix} \cdot \lambda} \cdot 100\,\% \tag{8}$$

The overall system gain G_S is determined by using Eq. (6). The irradiance E of the IS is measured using a calibrated photodiode with a reference to the National Standards situated in the same plane as the detector array. The measured QE (see Fig. 7) is calculated as a mean signal value over the number of pixels. The QE is very small. The reason is that in determining the QE, the fill factor was not taken into account.

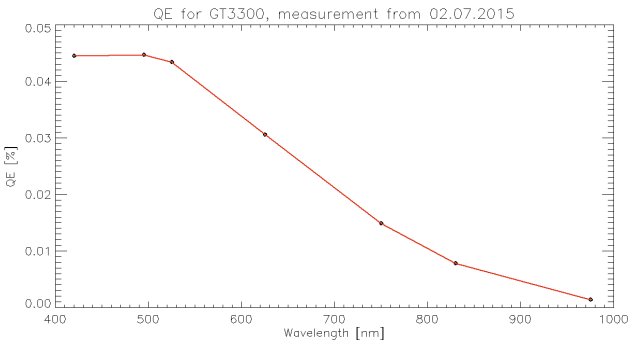

Fig. 7. Results for QE

4.5 Spectral Calibration

The spectral performance measurements and calibrations will be performed using Penray lamps. Figure 8 shows the spectral lines of the Ar(Hg)-Penray lamp measured in the BB focal plane using a camera with $5.5\,\mu\text{m} \cdot 5.5\,\mu\text{m}$ pixel size. The connection to the wavelengths can be found in the corresponding catalogs (see e.g. web-site [6,7]).

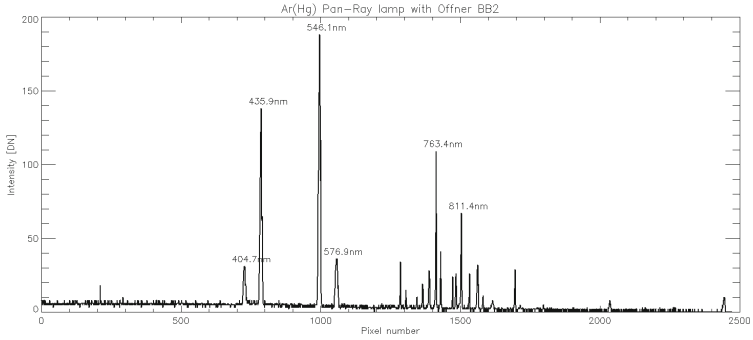

Fig. 8. Spectrum of the Ar Penray lamp measured in the DESIS focal plane

In Fig. 9 the linear relationship between the pixel position and the corresponding wavelength is shown. The deviation from the linear behavior (standard deviation) is 4 pixels (this corresponds to 2 nm in the wavelength region of 500 nm). This relationship also allows to determine the linear dispersion of the test setup. 500 nm are mapped to 1000 pixels on the chip (~ 0.5 nm/pixel).

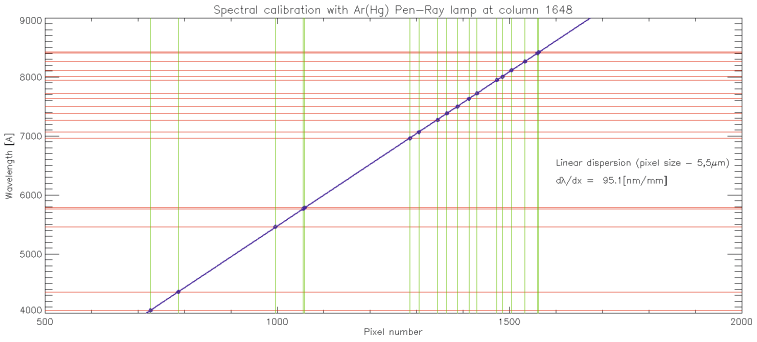

Fig. 9. Linear dependence between known wavelength and position on the chip. The linear dispersion is 95.1 nm/mm or 0.52 nm/pixel.

Individual spectral lines allow an investigation of the spectral resolution of the spectrometer. For evaluation we use an approach from Reulke [2] for determination of the spatial resolution of a camera. To determine the resolution the Rayleigh criterion is used. Instead of the Bessel function, the normal distribution (Gaussian) is employed. The Gaussian is characterized by the dispersion σ_λ. Resolution is then the distance between two normalized and superimposed normal distributions that have a minimum of 0.73. The sigma dependent distance is $2.84 \times \sigma_\lambda$. Therefore the resolution corresponds to three times σ_λ.

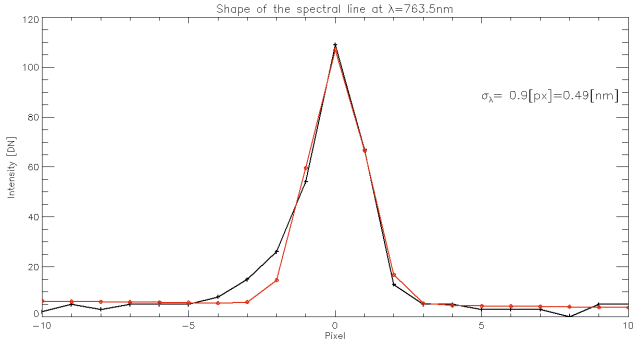

Fig. 10. Spectral distribution of the Ar-line at $\lambda = 736.5$ nm.

The following Fig. 10 shows the fit of a spectral line. The spectral resolution is about 1.5 nm. The dominant share is the telescope and the spectrograph. The pixel influence can be neglected. This can be explained from the square sum of the individual standard deviations. Assuming for the pixel on a $\sigma_{pix} = 0.5$, then it follows for the rest of the system $\sigma_{spec} = 0.8$ or 1.1. nm.

Table 2. Summary of calculated and measured parameter.

	System parameter	Measured values	Remarks
Optics			
f-Number $f_{\#}$	4		
Transmission	0.88		
Spectrometer			
Mirror reflection	0.92		
Grating efficiency	0.37		
Dispersion		0.523 nm/pixel	Sect. 4.5
Spectrom. slit	13 µm		
Detector			
Array	3296 × 2472		
Pixel size	5.5 µm × 5.5 µm		
Conversion gain		0.808 DN/e^-	Sect. 4.1
QE (522 nm)		0.0432 %	Sect. 4.4
Measurement condition			
Wavelength	522 nm		
Radiance (IS)	300 W/m^2 · µm · sr		
Integration time	1.4 s		
Results			
Signal	8290 DN	9090 DN	calculated
FWC at 2^{14} DN		$20Te^-$	see Sect. 4.2
SNR for $DN > 10^4$		≥ 100	
Dark current		4 e/s or 2.1 pA/cm^2	

5 Summary and Conclusion

The breadbord model of the DESIS instrument was tested, calibrations were carried out and performance data were verified. A summary of the measured parameter can be found in Table 2.

With the known system parameters and measured quantities in Table 2, allows the comparison of the measured and calculated signal. The incident radiance is known from the calibrated light source. Irradiance can calculated from

Eq. (1). The resulting number of electrons and conversion to digital numbers is related with Eq. 4. With optics transmission of $T_{opt} = 0.8778$ and mirror reflection $R_{mir} = 0.92$ the calculated signal is 8300 DN. The measured value is 9090 DN (see Fig. 4 at $\tau_{int} = 1.4$ ms).

It is worth noting that it is possible to calculate directly the expected signal from the known and measured parameters. It can also be derived parameters of the spectroscope, for example, the real resolution in spectral direction. Thus the design and future verification and calibration of DESIS can be carried out.

Acknowledgements. The authors would like to thank all the colleagues who have supported this work, especially Karl-Heinz Degen for performing the measurements.

References

1. Eckardt, A., Horack, J., Lehmann, F., Krutz, D., Drescher, J., Whorton, M., Soutullo, M.: DESIS (DLR Earth Sensing Imaging Spectrometer) for the ISS-MUSES platform. In: Proceedings of IEEE International Geoscience and Remote Sensing Symposium, IGARSS, Milano, Italy (2015)
2. Reulke, R., Sebastian, I.: Bestimmung der Bodenaufloesung der WAOSS-Kamera. Bild und Ton **45**, 271–275 (1992)
3. Kopeika, N.S.: A System Engineering Approach to Imaging. Morgan Kaufmann, SPIE Press Book, Bellingham (1998)
4. Janesick, J.R.: Scientific Charge-Coupled Devices. SPIE Press Book, Bellingham (2001)
5. Janesick, J.R.: Photon Transfer. SPIE Press Book, Bellingham (2007)
6. Optomechanics Research, Echelette Spectrograph. http://www.echellespectrographs.com/gallery.htm
7. L.O.T.-Oriel UK, Pen-Ray Line Sources. http://pas.ce.wsu.edu/CE415/PenRay_lamp_spectra.pdf
8. GT3300 camera from Allied. http://www.alliedvision.com/en/products/cameras/detail/3300.html
9. KAI-08050 Image Sensor. http://www.ccd.com/pdf/ccd_8050.pdf
10. Eckardt, A., Reulke, R., Schwarzer, H., Venus, H., Neumann, C.: sCMOS detector for imaging VNIR spectrometry. In: Proceedings of SPIE, vol. 8870 (2013)
11. Jahn, H., Reulke, R.: Systemtheoretische Grundlagen optoelektronischer Sensoren. Wiley-VCH, Berlin (2009)